



**HAL**  
open science

# Highly scannable injection seeded nanosecond Ti:sapphire ring laser

L. Cabaret, C. Drag

► **To cite this version:**

L. Cabaret, C. Drag. Highly scannable injection seeded nanosecond Ti:sapphire ring laser. European Physical Journal: Applied Physics, 2010, 51 (2), pp.20702. 10.1051/epjap/2010089 . hal-00609401

**HAL Id: hal-00609401**

**<https://hal.science/hal-00609401>**

Submitted on 19 Jul 2011

**HAL** is a multi-disciplinary open access archive for the deposit and dissemination of scientific research documents, whether they are published or not. The documents may come from teaching and research institutions in France or abroad, or from public or private research centers.

L'archive ouverte pluridisciplinaire **HAL**, est destinée au dépôt et à la diffusion de documents scientifiques de niveau recherche, publiés ou non, émanant des établissements d'enseignement et de recherche français ou étrangers, des laboratoires publics ou privés.

# Highly scannable injection seeded nanosecond Ti:Sapphire ring laser

L. Cabaret and C. Drag

Laboratoire Aimé Cotton, CNRS, bâtiment 505, Campus d'Orsay, 91405 Orsay Cedex, France

Received: date / Revised version: date

**Abstract.** A widely tunable injection seeded Ti:Sa ring cavity has been developed and characterized. The seeding source is a single mode quasi continuous wave Ti:Sa laser, continually tunable over more than  $2.5 \text{ cm}^{-1}$  (75 GHz). Its short term (pulse to pulse) stability is on the order of  $\pm 3.2 \text{ MHz}$  at a repetition rate of 20 Hz. The long term absolute stability is limited up to now to about  $\pm 10 \text{ MHz}$ . These frequency characteristics are transferred to the pulsed emission with minor degradations. The frequency chirps and shifts during the pulses are also studied using an optical heterodyne technique.

**PACS.** 42.55.-f Lasers – 42.60.-v Laser optical systems: design and operation – 42.60.Lh Efficiency, stability, gain, and other operational parameters

## 1 Introduction

High resolution laser spectroscopy, particularly molecular spectroscopy, requires single mode laser sources that cover a wide wavelength range and moreover that are continuously tunable over large frequency domains in a single run. A great part of the visible and near IR spectrum is easily covered by single mode CW lasers, such as dye lasers, Titanium:Sapphire (Ti:Sa) lasers, laser diodes, and more recently optical parametric oscillators (OPOs). Even the

UV side of the spectrum is attained by the use of highly efficient frequency doubling cavities, up to a wavelength of around 200 nm. However, solid state tunable CW lasers do not cover the entire domain (UV to near IR); large 'holes' remain, particularly between 500 and 680 nm, and even OPOs are not able up to now to replace completely visible dye lasers. Most favorable configurations associate OPO and frequency doubling, with an external cavity [1] or without [2]. Due to the high peak power of the laser emission, the pulsed mode allows us to have access to virtually any wavelength, from VUV to far IR, by the

use of nonlinear effects in various media. In fact, starting from a wide band laser medium such as Ti:Sa, this spectrum can be almost completely covered using more or less complicated mixing schemes. The oscillator linewidth is reduced if one inserts dispersing components inside the cavity. In a single mode CW cavity, the thinner selecting filter is generally a Fabry-Perot etalon. Obtaining a single mode emission from a pulsed cavity is less easy since the existence of a non homogeneous broadening behavior in the high gain transient regime permits the coexistence of many axial modes.

Therefore, rather than stacking filters, it is by far more efficient and cleaner to seed a pulsed cavity with a single mode, well frequency controlled, CW beam. Provided that the seeded frequency is matched (in phase) with one resonant mode of the pulsed cavity and that its amplitude greatly exceeds the spontaneous emission noise, all the fluorescence can be quenched inside this mode. In the optimum matching conditions, up to 99.8% of the pulsed emission intensity has been measured at the seeder frequency [3]. In return, for the conceptual simplicity of the configuration, several precautions must be taken concerning the beam alignment, the parameters adjustment (waist position and dimension) and the cavity length control. In the case of Ti:Sa pumped by a nanosecond pulse light, the cavity works in the gain switched regime so that the seeding is operated in its simplest form since there is no need for a Q-switch assembly.

Application domains of single mode nanosecond lasers are various and they are those that need highly coher-

ent beams. One of the most demanding experiment, in terms of spatial and temporal coherence, is population transfer in molecules by the use of a STIRAP scheme [4, 5]. The efficiency of the transfer to a selectively chosen level is directly linked to the quality of the beams coherence. In practice, one measures the spatial coherence for instance by propagating the laser beam through the focal zone of a lens and evaluating the quality factor  $M^2$ . This factor gives how many times the beam is from the diffraction limit. Measuring the temporal coherence is a more tedious task: the linewidth must be evaluated in the MHz range which corresponds to a resolution limit for most of the measuring methods. Global linewidth measurement methods sum in time all the physical broadening contributions, they include for instance the use of a high finesse Fabry-Perot interferometer for observing the Airy pattern broadening and make a deconvolution from the apparatus function. This method has been recently used by P. Dupré and T. A. Miller to measure the frequency pulse shape of a high energy injection seeded Ti:Sa laser [6]. Another powerful method makes use of a heterodyne technique to analyze the frequency drift during the pulse [7]. In an injection seeded scheme, the CW laser injector usually serves as a reference local oscillator to achieve the signal beating after frequency shifting by an acousto-optical device. With nanosecond duration pulses, the AO crystal needs to be high frequency modulated (typically at more than 200 MHz) in order to obtain enough sampling definition inside the pulse. Such a method has been extensively studied by R. T. White et al. to characterize

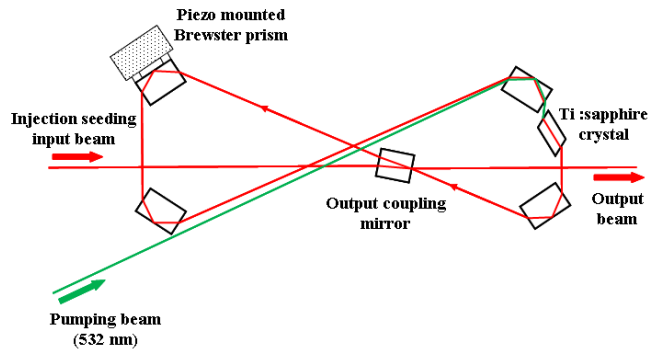
frequency chirps in OPOs injection seeded cavities [8–10] and by S. Hannamann et al. in a Ti:Sa oscillator-amplifier system [11].

We describe here a new ring cavity designed for an injection seeded Ti:Sa laser that is optimized for high resolution pulsed laser spectroscopy. The seeding laser is a tunable single-longitudinal-mode Quasi-Continuous-Wave (QCW) Ti:Sa with a large continuous scanning capability. Typically,  $2.5 \text{ cm}^{-1}$  (75 GHz) scans without mode hop are obtained and up to  $6 \text{ cm}^{-1}$  (180 GHz) scans can be attained in the most favorable spectral regions of the Lyot filter. The pulsed ring cavity is designed to reproduce the main spectral characteristics of the seeder, except the line-width that is nearly Fourier-transform limited. In particular, we demonstrate that the frequency stability and the scanning properties are transferred without appreciable degradation. The frequency chirp has been measured at different wavelengths thanks to an optical-heterodyne analysis technique and a direct fit method.

## 2 Experimental setup

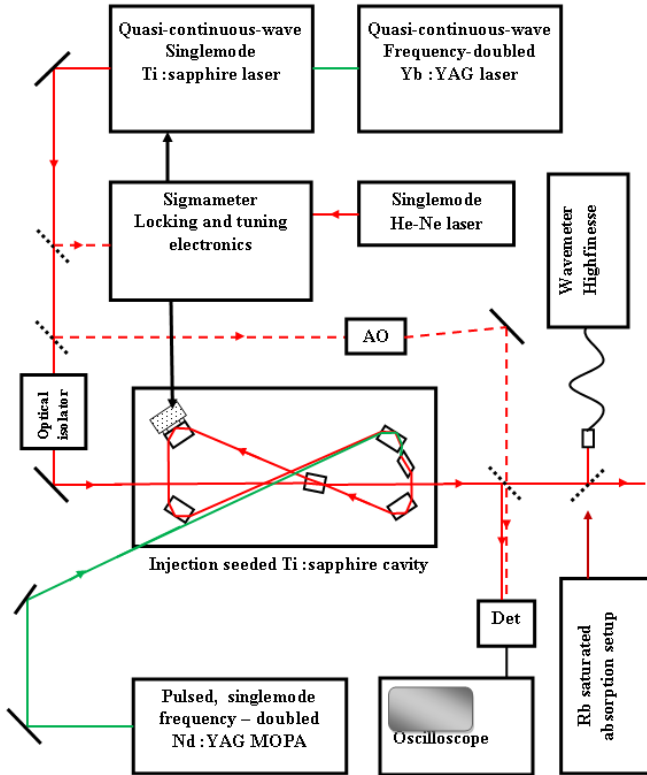
### 2.1 injection seeded pulsed ring cavity

Figure 1 displays a scheme of the injection seeded cavity. The original ring cavity arrangement is composed of four folding prisms in a X configuration, a Ti:Sa crystal and an output coupler. The prisms are BK7 rectangular parallelepipeds (12 mm x 18.25 mm thickness 6 mm) oriented in such a manner that the intra-cavity beam is incident at Brewster’s angle on the lateral faces and in total internal



**Fig. 1.** Scheme of the injection seeded ring cavity.

reflection on the back face. These prisms are equivalent to high-damage-threshold, quasi-achromatic and low-loss mirrors for the linear polarization in the plane formed by the ring cavity. One of them is mounted on a piezo actuator (Piezomechanik model PSt 150/20/18) in order to realize the frequency matching of one cavity mode to the injection seeded one. The output coupling is realized by reflection on a partially reflecting thick plate (diameter 12.7 mm, thickness 15 mm). The front face is anti-reflection coated in the range 700-1000 nm and the back face has a multilayer coating that is calculated to optimize the output coupling reflection with respect to the gain in the same spectral range; this function is more easily realized in a reflection mode than in a transmission mode which explains our choice. The seeded cavity is therefore a "in-line" setup for the Ti:Sa beam. The crystal is laser pumped by a home made master-oscillator power-amplifier frequency-doubled Nd:YAG laser delivering an energy of up to 30 mJ per pulse at a wavelength of 532 nm and at a repetition rate of 20 Hz with a pulse duration adjustable between 20 and 50 ns [12]; it was originally configured for the pumping of single mode optical parametric oscillators, and the output



**Fig. 2.** Overall setup of the tunable injection seeded Ti:Sa laser chain. The picture includes the sigmometer and the single-mode laser for long term stabilization. The wavemeter and the Rb saturated absorption setup are used for the frequency measurements.

beam has a nearly Gaussian profile after amplification and frequency doubling.

The pumping beam is introduced through one of the Brewster prisms so that the Ti:Sa crystal is pumped in an almost collinear configuration with respect to the cavity axis taking account of the small dispersion angle at the crystal input. Generally, that situation is not a real drawback since it only decreases a little bit the output energy. However, we will see that in our case the non-collinear pumping limits the tunability towards the infrared part of the spectrum. The Ti:Sa crystal is a Brewster cut slab of

cross section 5 mm x 7 mm and 15 mm length (from Saint Gobain / Roditi); its doping concentration is 0.15% which leads to a nominal absorption coefficient of  $2.1 \text{ cm}^{-1}$  at 532 nm.

## 2.2 Overall setup

Figure 2 illustrates the setup of the laser system with its locking and tuning electronics. The apparatus for frequency characterization is also shown. The injection seeding laser is composed of a quasi-continuous-wave (QCW) frequency-doubled Yb:YAG pumping laser ( $\lambda = 515 \text{ nm}$ ) [13] followed by a QCW Ti:Sa laser, tunable in the range 725-960 nm. This laser emits single-axial-mode gain-switched pulses of 150-200  $\mu\text{s}$  duration at a repetition rate of 20 Hz; the laser cavity and the locking system are described in reference [14]. In the present version, the intracavity  $\text{LiNbO}_3$  electro-optic Fabry-Perot etalon has been replaced by a RTP ( $\text{RbTiOPO}_4$ ) solid etalon that is less subject to piezo-acoustic perturbations. After a short period of relaxation oscillations (20  $\mu\text{s}$ ) at the beginning of the pulse, the laser power increases smoothly up to the steady-state regime that is generally reached at the end of the pulse (figure 3). The pulse building time depends mainly on the pumping power and on the output wavelength.

Short time stabilization is obtained by servo-locking the QCW Ti:Sa laser frequency on a static sigmometer (phase quadrature Michelson interferometer) [16]. We modified the electronic setup to use this interferometer in quasi-continuous regime. For the long term stabilization, the sigmometer itself has its optical path difference servo-locked

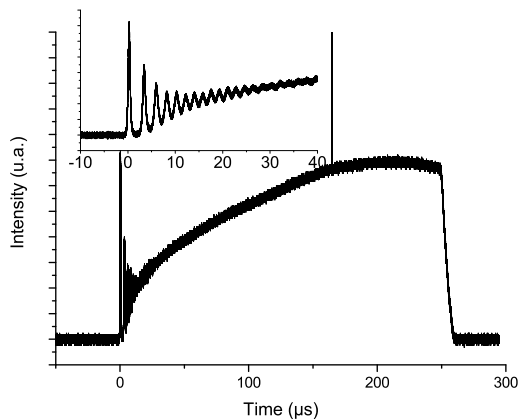


**Fig. 3.** Temporal evolution of the pulse shape of the QCW Ti:Sa laser. Inset : relaxation oscillations at the beginning of the pulse.

with a dual polarization stabilized He-Ne laser (Coherent model 200) with an nominal absolute accuracy of  $\pm 3$  MHz. The wavelength is measured with an lambdameter (Angstrom WS-8) calibrated by a rubidium saturated absorption setup. In QCW regime, the accuracy of the wavenumber so measured is  $\pm 0.8$  mK. In pulsed regime, the lambdameter permit us to verify the single longitudinal mode operation and gives a mean value of the seed wavelength with a precision of about 1 mK.

### 3 Frequency characterization

#### 3.1 Quasi-continuous lasers (QCW)

The frequency stability and the tuning characteristics of the injection seeding laser are of major importance to manage properly the frequency of the pulsed laser. To this end, we have fully characterized its emission. The single axial mode nature of the laser beam is monitored by the

use of an electro-optically scanned confocal Fabry-Perot interferometer [14]. When the laser is in a stable configuration, i.e. when the transmission maxima of the wavelength selection filters are exactly superimposed, we verified that the emission is always single mode over the full pulse duration. Spurious mode hops appear only if the cavity is unlocked or at the end of long scans. The main drawback is probably the transient frequency shift during the pulse that was previously underlined and measured in Nd:YAG and Yb:YAG QCW lasers [13,14]; the shift was identified as an effect of thermal deposition inside the pumped volume. In the case of Ti:Sa, two parameters tend to increase the shift: first, the large quantum defect between the energies of pumping and laser photons so that more power is lost in the crystal, and second, the high power density of the pumping beam. However, since the thermal diffusivity of the Sapphire host is higher than YAG's one, the measured frequency shift is no longer linear. An accurate analysis of the transient frequency shift in the case of a Ti:Sa QCW laser will be published elsewhere. The residual measured frequency chirp is around 10 MHz in our experimental conditions.

Fortunately, the pulse to pulse repetability of the chirp evolution is excellent so that the seeded (nanosecond) laser will be only sensitive to the natural global frequency jitter of the QCW laser, provided the Q-switched pumping laser is triggered at a constant delay with respect to the front edge of the QCW Yb:YAG pumping pulse (see Fig. 3).

Using the sigmometer, the frequency fluctuations of the QCW Ti:Sa laser are reduced but we observe an ap-

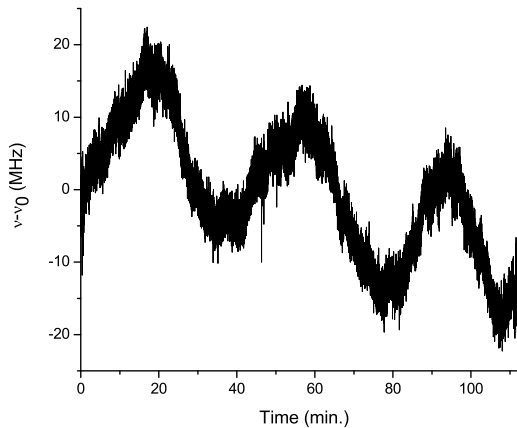


**Fig. 4.** Long term frequency fluctuations of the QCW Ti:Sa laser when locked to a sigmameter. The absolute wavelength during the acquisition is around 810 nm.

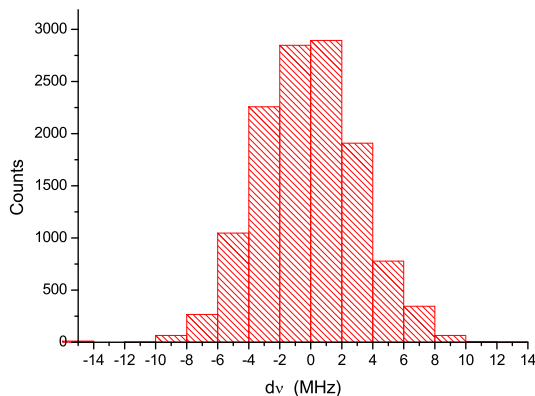


**Fig. 5.** Pulse to pulse frequency jitter distribution over a sequence of 1000 pulses. The QCW Ti:Sa laser is locked to the sigmameter.

preciable degradation as it is shown on figure 4. The long term frequency decrease is probably due to a slow drift of the wavemeter. The large amplitude oscillations ( $\pm 10$  MHz) are connected to the temperature variations in the clean room. They are caused by the difference in sensitivity to the temperature of air refraction index, inside the interferometer, between the He-Ne and Ti:Sa wave-

lengths. Working the interferometer under vacuum should solve this problem.

The short term (shot to shot) frequency jitter appears on figure 4 as a "thickening" of the trace and the peak to peak value that could be deduced from this recording is roughly  $\pm 3.5$  MHz. However, such a value cannot be considered as reliable because the wavemeter resolution is of the same order ( $\pm 2$  MHz) and measurements over several shots are averaged to calculate the frequency. A more reliable result is achieved if one records the phase informations delivered by the sigmameter. The two signals in phase quadrature detected at the output of the sigmameter are of the form:  $I_0(1 + \cos 2\pi\sigma d)$  and  $I_0(1 + \sin 2\pi\sigma d)$ , where  $I_0$  is proportional to the input laser intensity,  $\sigma$  is the wave number and  $d$  is the optical path difference between the two arms of the interferometer ( $l_{opt}$  is the one way optical length difference):  $d = 2l_{opt}$ . After electronic subtraction of the bias and division by  $I_0$ , we have access to the phase  $\phi$  through the measured cos and sin signal values. A  $2\pi$  phase variation corresponds to a change  $\Delta\nu = c/2l_{opt}$  of the laser frequency. The long arm length of the interferometer is chosen such a way that residual frequency variations have a low amplitude compared to  $\Delta\nu$ . The pulse to pulse frequency jitter  $d\nu$ , around a reference frequency  $\nu_0$ , is calculated from the phase variation  $d\phi$  measured at each pulse:  $d\nu = \Delta\nu(d\phi/2\pi)$ . A recording of  $d\nu$  in a sequence of 1000 pulses is displayed on figure 5. The nearly Gaussian curve distribution leads to a standard deviation of 3.23 MHz.

A fine frequency tuning of the laser is realized through the piezo mounted mirror by applying a slow voltage ramp. Large scans are obtained if rapid returns of exactly an integer of the cavity free spectral range are induced on the piezo. The ramp returns are triggered just after a laser pulse in such a way that the locking loop does not "see" the cavity mode change. Since the reset time is short ( $\approx 2$ ms) compared to the shot period (50 ms), the laser frequency is not perturbed and the scan is quite linear. One can produce scans as large as  $6 \text{ cm}^{-1}$  (180 GHz) for some favourable positions of the Lyot filter; however, scans of  $2.5 \text{ cm}^{-1}$  are more routinely obtained as shown on figure 6 where a single mode hop can be clearly seen. The measurement is done with the pulsed seed laser.

The power needed to seed the pulsed cavity with a high efficiency is low, typically in the mW range [3]. However, injection locking can be effective even very far from the free running wavelength if a high power seeding signal is employed. In our case we measured a peak power of 1 watt at the output of the QCW Ti:Sa laser ( $\lambda = 810 \text{ nm}$ ) when it is pumped by 10 watts peak power from the Yb:YAG QCW laser. As we shall see later, this will ensure a large locking range without the need of additional wavelength selection filters. The cavity has also to be locked in phase with the injected beam.

### 3.2 Pulsed laser

The frequency characterization of the pulsed singlemode emission has also been realized in two ways: a global absolute frequency measurement (with the lambdameter for

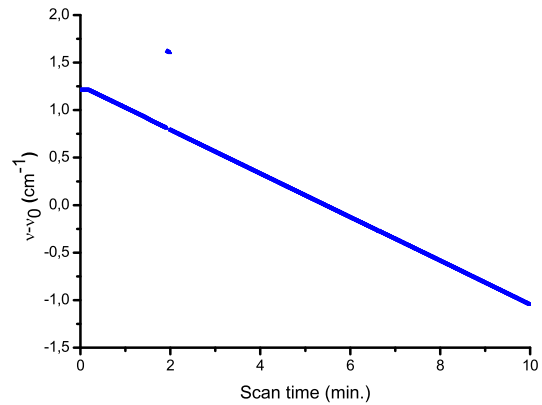


**Fig. 6.** Linear frequency tuning of the pulsed injection seeded cavity ( $2.5 \text{ cm}^{-1}$ ). A single mode hop is clearly seen.

example) and a chirp analysis during the pulse. The wavemeter is able to give an absolute value of the laser frequency (at peak intensity) with a precision of  $\pm 10 \text{ MHz}$  in pulsed mode as recorded in Fig. 6. However, this apparatus cannot give indications about the frequency evolution during the pulse. To analyse the chirp, we employed an optical heterodyne method largely developed by several groups, in particular by R. T. White et al. [8]. In our setup, the QCW Ti:Sa laser serves as a local oscillator; the beam passes (one way) through an acousto-optic Bragg modulator that is modulated at a frequency  $f_m$  of 200 MHz. The frequency shifted QCW beam and the unshifted pulsed beam are superimposed on a fast detector (EOT model ET-2020) and the beating signal is acquired by a TDS5104 Tektronics scope having a 1 GHz analogic bandpass and a 5 Gsample/s numeric sampling rate. Figure 7.a gives a typical beating signal at a wavelength corresponding to the center of the free running cavity emission band. The "instantaneous" frequency chirp is extracted from the de-

tected signal  $V(t)$  in the following manner. Let  $E_{QCW}$  be the amplitude (constant over the pulse duration) of the QCW laser field and  $E_P(t)$  be the amplitude of the pulsed laser field; the beating signal satisfies to the proportionality relation:

$$V(t) \propto 2E_{QCW}E_P(t) \cos(\omega_m t + \phi(t)) \quad (1)$$

Where  $\omega_m = 2\pi f_m$  is the angular frequency. Multiplying  $V(t)$  by  $\cos(\omega_m t)$  and then  $\sin(\omega_m t)$  gives the two relations:

$$V(t) \cos(\omega_m t) \propto E_P(t)[\cos\phi(t) + \cos(2\omega_m t + \phi(t))] \quad (2)$$

$$V(t) \sin(\omega_m t) \propto E_P(t)[\sin(2\omega_m t + \phi(t)) - \sin\phi(t)] \quad (3)$$

This allows us to get back to the amplitude  $E_P(t)$  and to the "instantaneous" phase  $\phi(t)$  after elimination of the terms at the modulation frequency. For this purpose a numerical filter at a frequency  $f_c = f_m/4$  is applied to the functions (2) and (3) so that the remaining terms are proportional to  $E_P(t) \cos\phi(t)$  and  $-E_P(t) \sin\phi(t)$ . The "instantaneous" frequency shift  $f_{inst}(t)$  is directly obtained using:  $f_{inst}(t) = 1/2\pi \times d\phi(t)/dt$ .

Figure 7.b shows the reconstructed intensity and the calculated instantaneous frequency shift. In this particular situation (near the maximum of the gain curve), the total frequency chirp is negligible. On the contrary, when the seeded wavelength is far from this maximum, an important chirp is measured (cf. Fig. 8). This kind of frequency shift was analysed in dye amplifiers [17], in OPOs [9] and Ti:Sa [6, 11]. While in a non-linear medium the shift is primarily due to the phase mismatch between the interacting waves, in fluorescent media it is the gain dependence

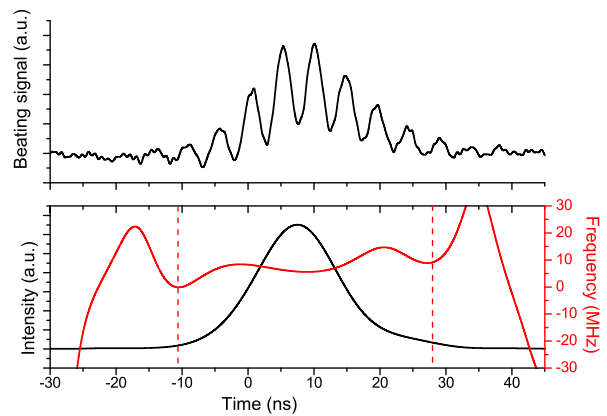


**Fig. 7.** a) Typical beating signal between the shifted QCW Ti:Sa and the pulsed seeded Ti:Sa. b) Recalculated intensity and "instantaneous" frequency in the case of a seeding at the maximum of the gain curve. The noise at the rising and falling edges of the pulse is due to the filtering process used in the calculation. Vertical bars indicate approximately the validity domain of the measurement.

of the refractive index, because of the varying population inversion density that is responsible for the frequency distortions. The elimination (or at least the minimization) of the frequency shift is straightforward in the case of an OPO since one must only take care to adjust the phase matching condition in the crystal for the exact injection seeded wavelength. In the case of a fluorescent medium, the "instantaneous" frequency  $f_{inst}$  can be related to the population density  $N_1(t)$  of the excited state. In the case of dye amplifier, an analytical model is developed by Melikechi et al. [17]. For an amplifier of length  $L$ , the evolution of the "instantaneous" frequency is given in low gain approximation by:

$$f_{inst}(L, t) = f_{inst}(0, t) - \frac{L}{2n(\nu)\lambda} \alpha'(\nu) \frac{d}{dt} N_1(t) \quad (4)$$

where  $n(\nu)$  and  $\alpha'(\nu)$  are the refractive index and polarizability. The source of frequency shifts in the amplifier is linked to the rate of change of population density, or, equivalently, the rate change of the gain. So the frequency chirp may be null only at the maximum of the gain curve where the real part of the polarizability  $\alpha'(\nu)$  is zero. However, the dynamical behavior of Ti:Sa is somewhat different from dye's one due to its much longer fluorescent life time, almost three orders of magnitude. In a dye solution, for typical pulse durations of 10 to 20 ns, the time evolutions of the pumping pulse and of the gain are almost synchronized leading to a dispersion-like curve for  $f_{inst}$ . In a Ti:Sa amplifier working in the gain switched regime, the gain is already at its maximum when the laser pulse starts growing so that the gain decreases all along the pulse duration. Consequently, the chirp seen by the detection system corresponds only to the central part of the dispersion curve. The polarizability  $\alpha'(\nu)$  is positive on the blue side of the gain curve, and it is negative on the red side. As just mentioned, the term  $\frac{dN_1(t)}{dt}$  is always negative so that the chirp is positive if the injected wavelength is in the blue part of the gain curve and negative in the red part. For the comparison with our experiment, it is necessary to note that, due to the presence of the output coupler, the free running wavelength (770 nm) does not coincide with the peak of the gain curve (790 nm). However, the null chirp is rather localized at 790 nm which confirms the predominance of the electric susceptibility parameter. We present a record of the chirp in the figure 8 where the

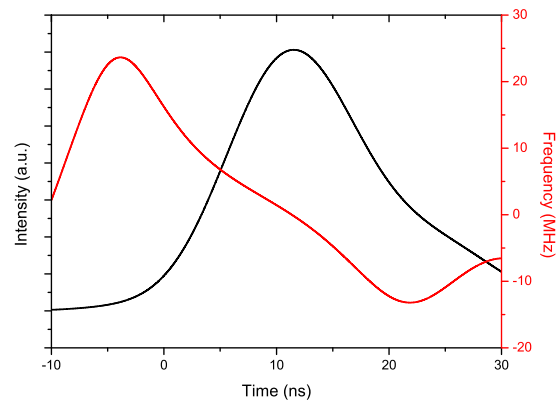


**Fig. 8.** Measured intensity and "instantaneous" frequency for an injected beam at 810 nm. The chirp is about 30 MHz during 20 ns.

wavelength is around 810 nm, i.e. 40 nm redder than the free running wavelength.

Thanks to the high power of the QCW seeding source, the injection seeding is achieved with a high efficiency far outside the free running bandwidth of the laser. The total seeding range of the cavity is therefore nearly 100 nm without any wavelength selection filter inside the cavity. To enlarge the single mode spectral range, the use of a coarse selector is necessary in order to force the free running laser emission to reach the desired wavelength. We have tried a one plate (0.5 mm thick) Lyot filter that allows us to cover the range 700-810 nm. However, the red part of the spectrum (810 - 1000 nm) has never been reached although the cavity was originally designed to cover the whole spectral emission band of the Ti:Sa. Actually, when the Lyot filter is inserted in the cavity, the scanned range is reduced to the blue part of the spectrum as the result of three combined effects: the shape of the gain spectral curve, the

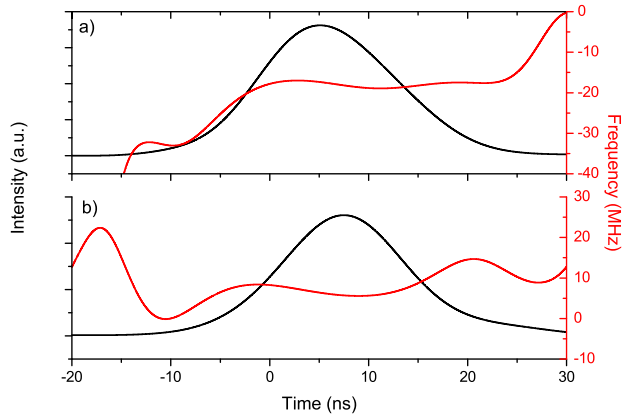


**Fig. 9.** Measured intensity and "instantaneous" frequency for an injected beam at 793 nm. The chirp is negligible because the emitted wavelength is around the peak of the gain curve (790 nm). The cavity pulling effect is observed in both cases : when the cavity is red detuned (a) or blue detuned (b) from the seeder frequency.

reflectivity curve of the output coupler and the mode interval of the birefringent plate. Clearly the lowest threshold wavelength is never located beyond 810 nm. This drawback is stressed by a geometrical effect due to the four mirror configuration of the cavity [x]; for any wavelength, a particular angle of propagation inside the crystal can be found for which the cavity is perfectly adjusted. In the range 700-1000 nm, this dispersion angle is only  $\pm 20$  arc min so that we can consider that at each wavelength, the propagation in the crystal is always nearly oriented along the maximum gain axis: the cavity adjustments (tilts or translation of the mirrors) cannot achieve a wavelength selection, in other words any action on the cavity parameters will not change the free running wavelength.

Locking the cavity length to keep a cavity axial mode in resonance with the injected QCW mode might be done by using conventional methods (i.e. Hänsch-Couillaud [18] or Pound-Drever-Hall [19] methods). These technics are very effective, and fast, in continuous wave regime. In a low duty cycle pulsed operation, the lack of information between the pulses does not permit to use fast time constants and the locking can be obtained by a simpler method. Consequently, we simply detect here the ring interference system created at the cavity output by the natural expansion of the injected beam inside the plane/plane cavity. The detector is placed on the edge of the central spot in such a way that, around the resonance, the detected interference signal has a large slope with respect to a length variation. Just before each pumping pulse, a sample and hold component pick-up a selected signal value that is compared to an adjustable bias voltage. The bias value is chosen in order to lock the cavity mode on resonance exactly. The overall time constant of the gain loop is on the order of 500 ms so that slow thermal length variations are well corrected. However, a pulse to pulse jitter is inevitable and cumulative frequency drifts arise first from the seeder jitter itself as analysed above and second from cavity-pulling effects when the injection seeded and cavity mode frequencies are slightly shifted. Inside an injection seeded cavity, it is known that the output frequency is pulled to the nearest axial mode of the bare cavity, so that finally the external signal does not determine the exact output frequency. The observed shift during the pulse, between the injected and emitted frequencies, is then a

combined effect of the rate change of the gain chirp and of the pulling drift. An example of these shifts is presented in the figure 9. Cavity pulling effects in injection seeded cavities have been examined by M. S. Bowers and S. E. Moody [20] where simulations show clearly that the output pulse frequency is determined by the pulse laser oscillator. Note that the emitted frequency is the nearest axial mode of the resonator from the seeder frequency.

## 4 Conclusion

We described a novel scheme for an injection seeded Ti:Sa ring cavity widely tunable over  $2.5 \text{ cm}^{-1}$ . The QCW seeding Ti:Sa and pulsed lasers have been characterized. The long term ( $\pm 10 \text{ MHz}$ ) and short term ( $\pm 3,2 \text{ MHz}$ ) stabilities of the QCW Ti:Sa are transferred to the pulsed cavity. An optical heterodyne technique allows us to measure frequency chirps and shifts during the pulses. We have clearly shown that in a Ti:Sa amplifier, as already demonstrated in dye lasers, the frequency chirp is caused by the transient time evolution of the gain during the pulse. The instantaneous frequency increases when the injected wavelength is in the blue part of the gain curve, decreases in the red part and is almost stationary at the maximum of the gain curve. Cavity pulling effects have also been observed.

## References

1. Schneider, K. and Kramper, P. and Schiller, S. and Mlynek, J., *Opt. Lett.* **22**, (1997) 1293-1295.
2. Melkonian, J.M. and My, T.H. and Bretenaker, F. and Drag, C., *Opt. Lett.* **32**, (2007) 518-520.
3. K. Ertel, H. Linné, and J. Bösenberg, *Appl. Opt.* **44**, (2005) 5120-5126.
4. U. Gaubatz, P. Rudecki, S. Schiemann and K. Bergmann., *J. Chem. Phys.* **92**, (1990) 5363.
5. S. Schiemann, A. Kuhn, S. Steuerwald and K. Bergmann., *Phys. Rev. Lett.* **71**, (1993) 3637.
6. P. Dupré and T.A. Miller, *Rev. Sci. Instrum.* **78**, (2007) 033102.
7. Fee, M.S. and Danzmann, K. and Chu, S., *Phys. Rev. A* **45**, (1992) 4911-4924.
8. R. T. White, Y. He, B. J. Orr, M. Kono, and K. G. H. Baldwin, *J. Opt. Soc. Am. B* **21**, (2004) 1577-1585.
9. R. T. White, Y. He, B. J. Orr, M. Kono, and K. G. H. Baldwin, *J. Opt. Soc. Am. B* **21**, (2004) 1586-1594.
10. R. T. White, Y. He, B. J. Orr, M. Kono, and K. G. H. Baldwin, *J. Opt. Soc. Am. B* **24**, (2007) 2601-2609.
11. S. Hannemann, E.-J. Van Duijn, and W. Ubachs, *Rev. Sci. Instrum.* **78**, (2007) 103102.
12. L. Cabaret and C. Drag, *Eur. Phys. J. Appl. Phys.* **37**, (2007) 65-72.
13. L. Cabaret, *Appl. Phys. B* **94**, (2009) 71-79.
14. L. Cabaret, P. Camus, R. Leroux, and J. Philip, *Opt. Lett.* **26**, (2001) 983-985.
15. L. Cabaret, J. Philip, and P. Camus, *IEEE J. Quantum Electron.* **36**, (2000) 1323-1332.
16. P. Juncar, J. Pinard, *Opt. Commun.* **14**, (1975) 438-441.
17. N. Melikechi, S. Gangopadhyay, and E. E. Eyler, *J. Opt. Soc. Am. B* **11**, (1994) 2402-2411.
18. T.W. Hänsch, B. Couillaud, *Opt. comm.* **35**, (1980) 441-444.

19. R.W.P. Drever, J.L. Hall, F.V. Kowalski, J. Hough, G.M. Ford, A.J. Munley, H. Ward, *Appl. Phys. B* **31**, (1983) 97-105.
20. M. S. Bowers, S. E. Moody, *J. Opt. Soc. Am. B* **11**, (1994) 2266-2275.